Electronic Supplementary Material (ESI) for Nanoscale.
This journal is © The Royal Society of Chemistry 2023

Supplementary Information, SI I, for

Crystalline Restacking of 2D-Materials from their Nanosheets Suspensions

Lina Cherni,[1] Karin El Rifaii,[2] Henricus H. Wensink,[2*] Sarah M. Chevrier,[1] Claire Goldmann,[2] Laurent J. Michot,[3] Patrick Davidson,[2*] Jean-Christophe P. Gabriel,[1*]

1 Université Paris-Saclay, CEA, CNRS, NIMBE-LICSEN, 91191 Gif-sur-Yvette, France.

2 Laboratoire de Physique des Solides, Université Paris-Saclay, CNRS, 91405 Orsay, France.

3 Laboratory of Physical Chemistry of Electrolytes and Interfacial Nanosystems (PHENIX), Sorbonne Université, CNRS, 75005 Paris, France.

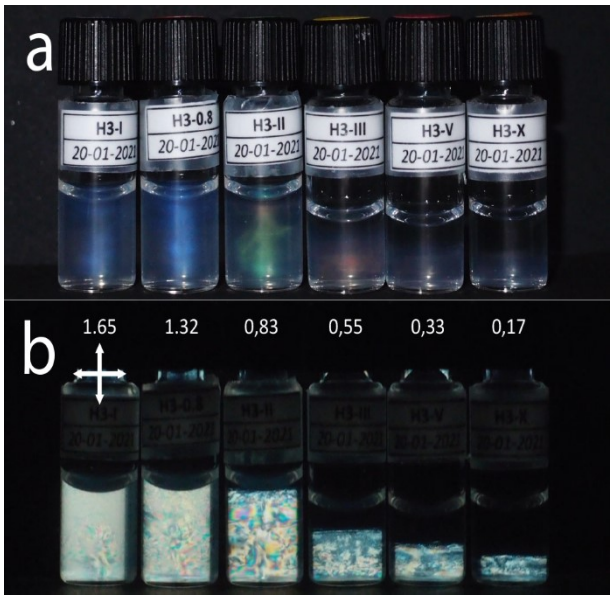

Figure SI 1. Photographs of a series of sample tubes with $H_3Sb_3P_2O_{14}$ weight fraction decreasing from left to right: 1.65, 1.32, 0.83, 0.55, 0.33, and 0.17 %w/w observed (a) in natural light and (b) between crossed polarizers.

Figure SI 2. A typical scanning electron microscopy (SEM) image of $H_3Sb_3P_2O_{14}$ nanosheets.

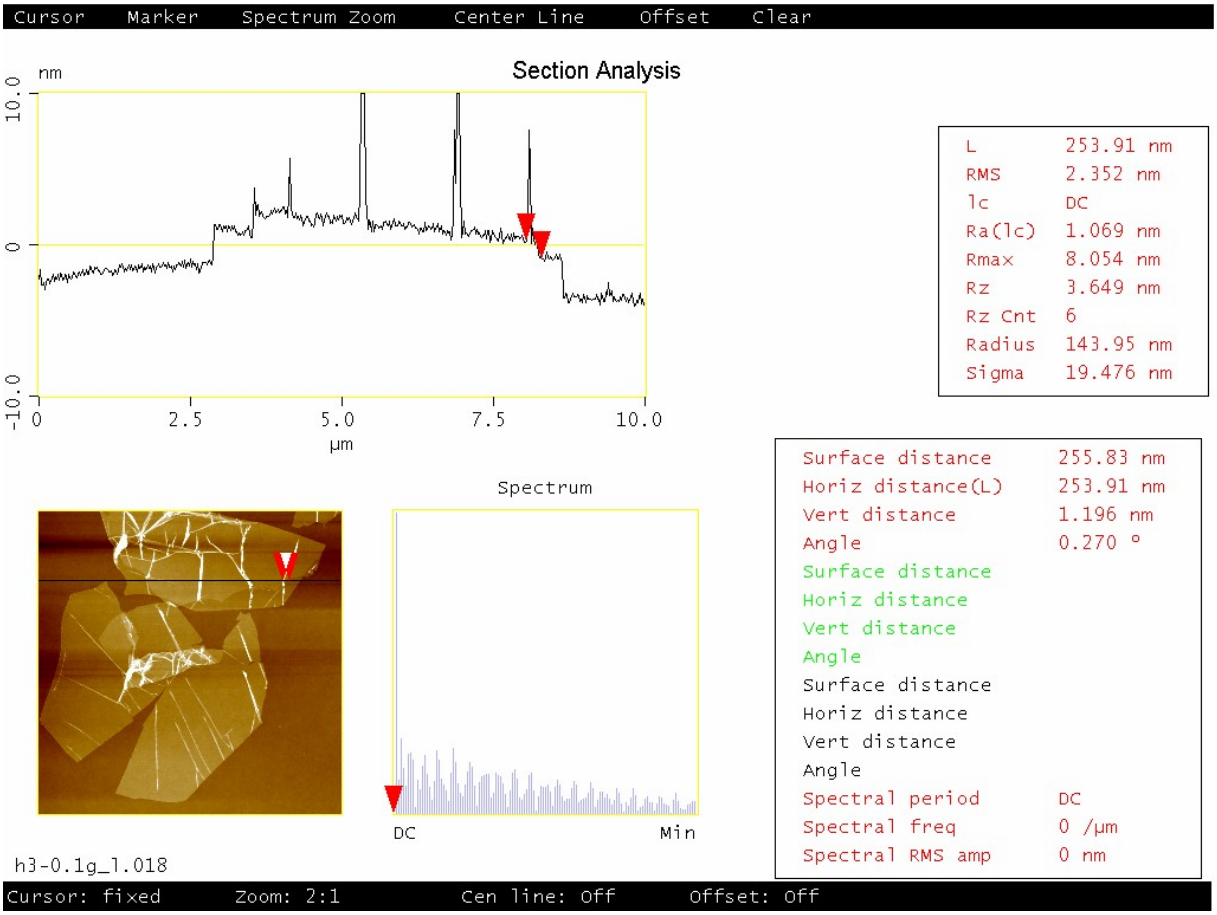

Figure SI 3. A typical atomic force microscopy (AFM) image of $H_3Sb_3P_2O_{14}$ nanosheets with a horizontal cut showing that the nanosheet thickness is ≈ 1.2 nm.

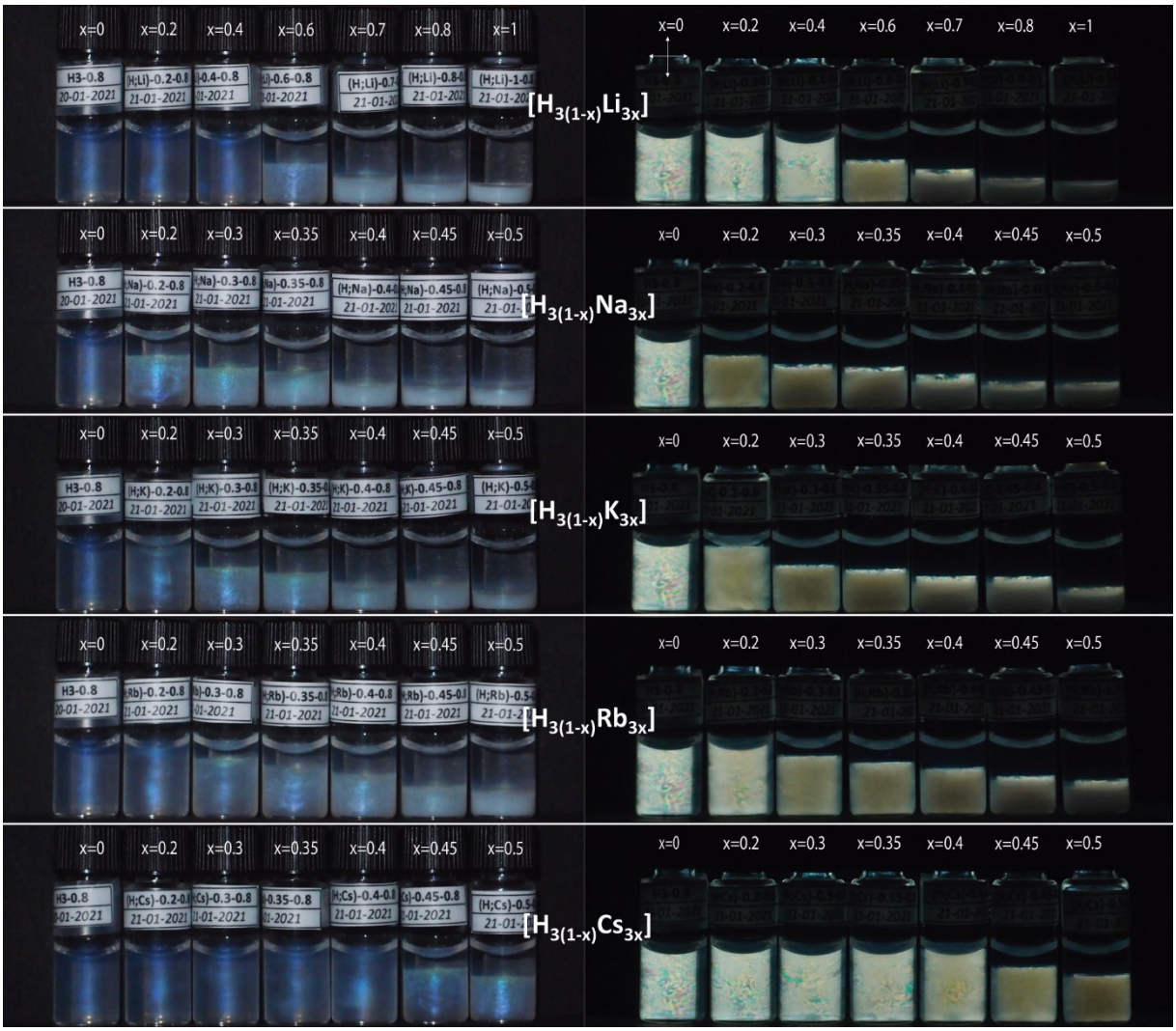

Figure SI 4. Photographs of five series of sample tubes observed in natural light (right) and between crossed polarizers (left). For each series, the $H_{3(1-x)}M_{3x}Sb_3P_2O_{14}$ nanosheet weight fraction is kept constant (1.32 %w/w) but the x value corresponding to the alkaline cation increases from left to right: x = 0, 0.2, 0.4, 0.6, 0.7, 0.8, and 1 for Li+ and x = 0, 0.2, 0.3, 0.35, 0.4, 0.45, and 0.5 for the other cations (Na^+, K^+, Rb^+, Cs^+).

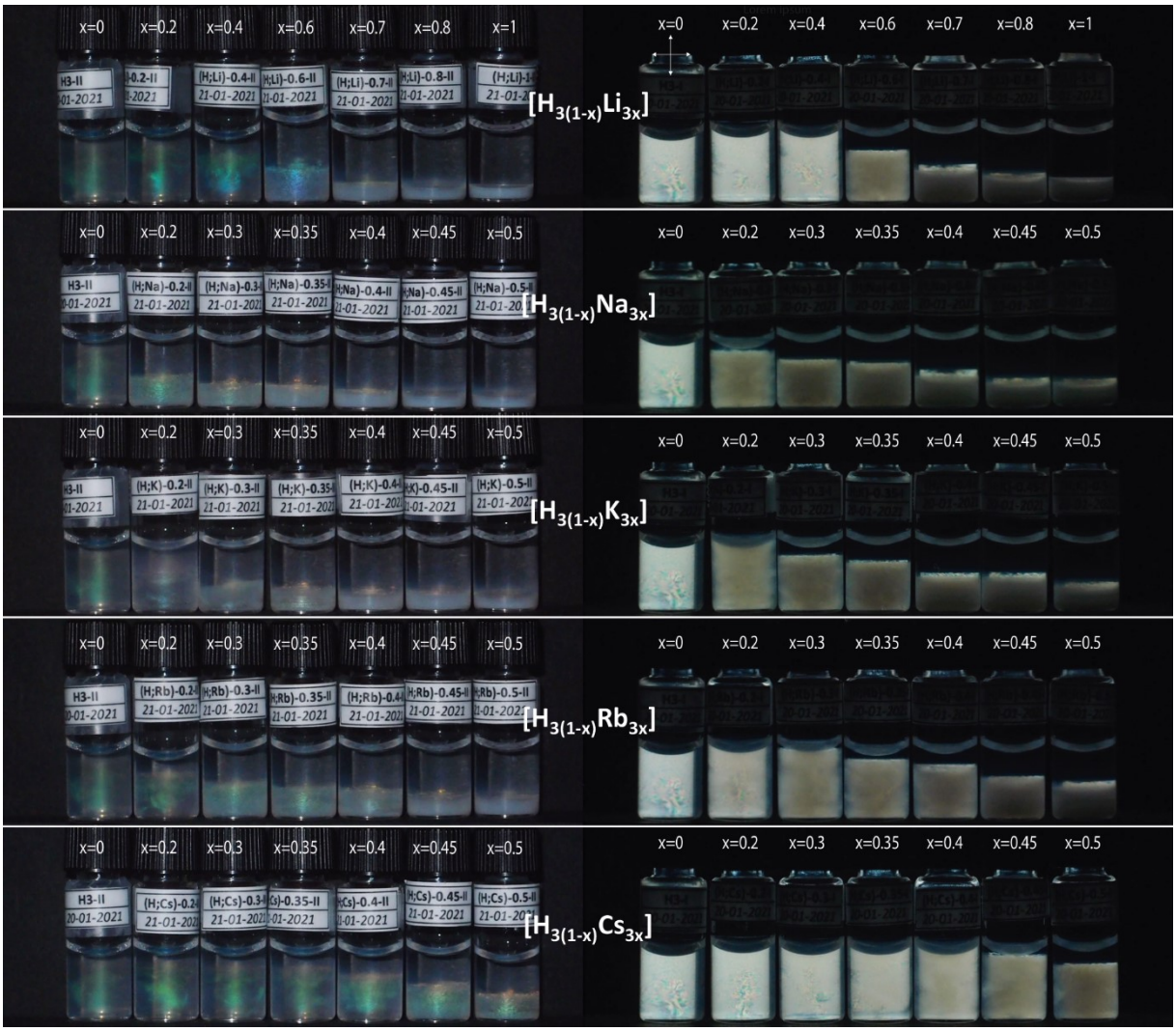

Figure SI 5. Photographs of five series of sample tubes observed in natural light (right) and between crossed polarizers (left). For each series, the $H_{3(1-x)}M_{3x}Sb_3P_2O_{14}$ nanosheet weight fraction is kept constant (0.83 %w/w) but the x value corresponding to the alkaline cation increases from left to right: x = 0, 0.2, 0.4, 0.6, 0.7, 0.8, and 1 for Li^+ and x = 0, 0.2, 0.3, 0.35, 0.4, 0.45, and 0.5 for the other cations (Na^+, K^+, Rb^+, Cs^+).

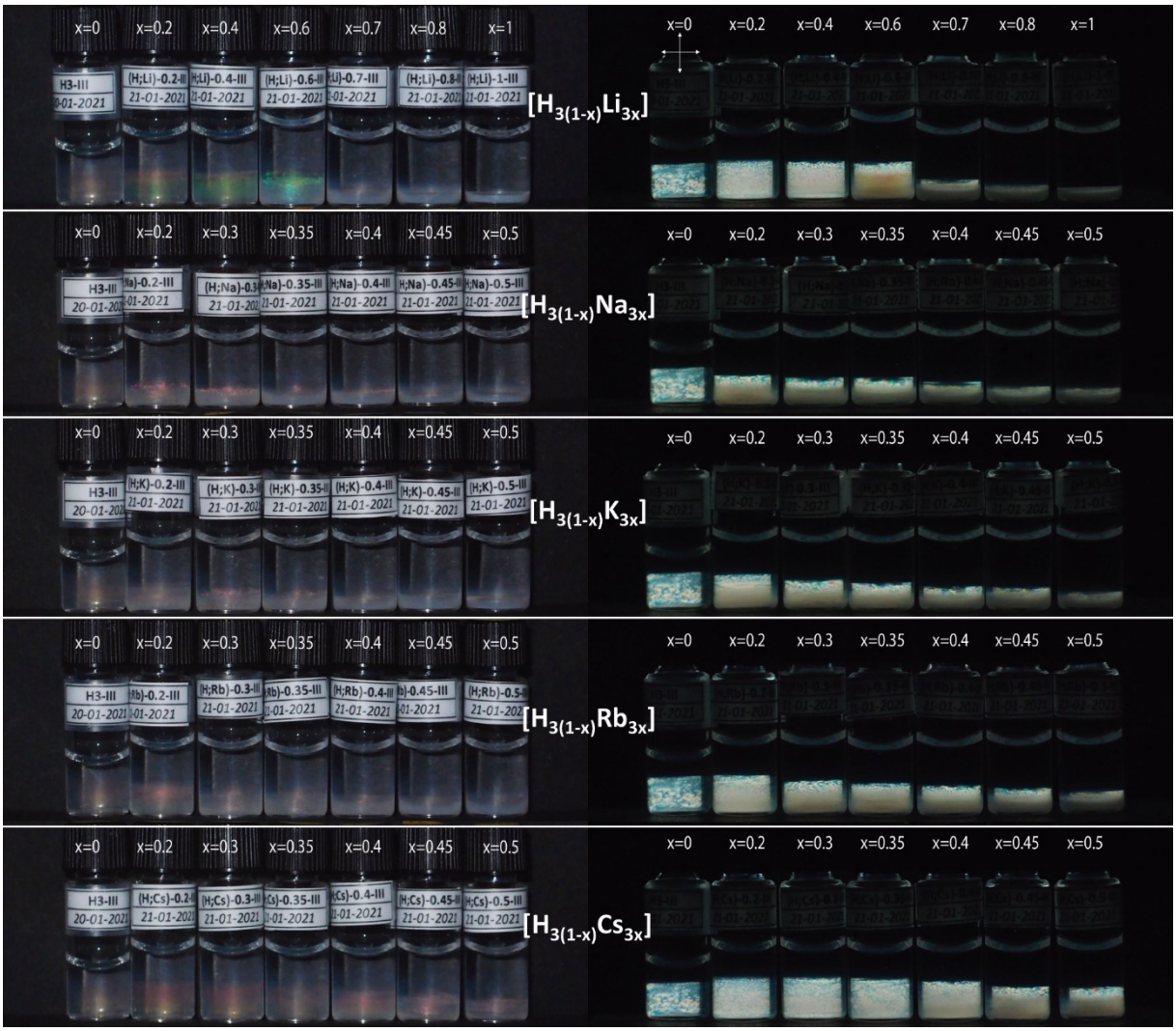

Figure SI 6. Photographs of five series of sample tubes observed in natural light (right) and between crossed polarizers (left). For each series, the $H_{3(1-x)}M_{3x}Sb_3P_2O_{14}$ nanosheet weight fraction is kept constant (0.55 %w/w) but the x value corresponding to the alkaline cation increases from left to right: x = 0, 0.2, 0.4, 0.6, 0.7, 0.8, and 1 for Li^+ and x = 0, 0.2, 0.3, 0.35, 0.4, 0.45, and 0.5 for the other cations (Na^+, K^+, Rb^+, Cs^+).

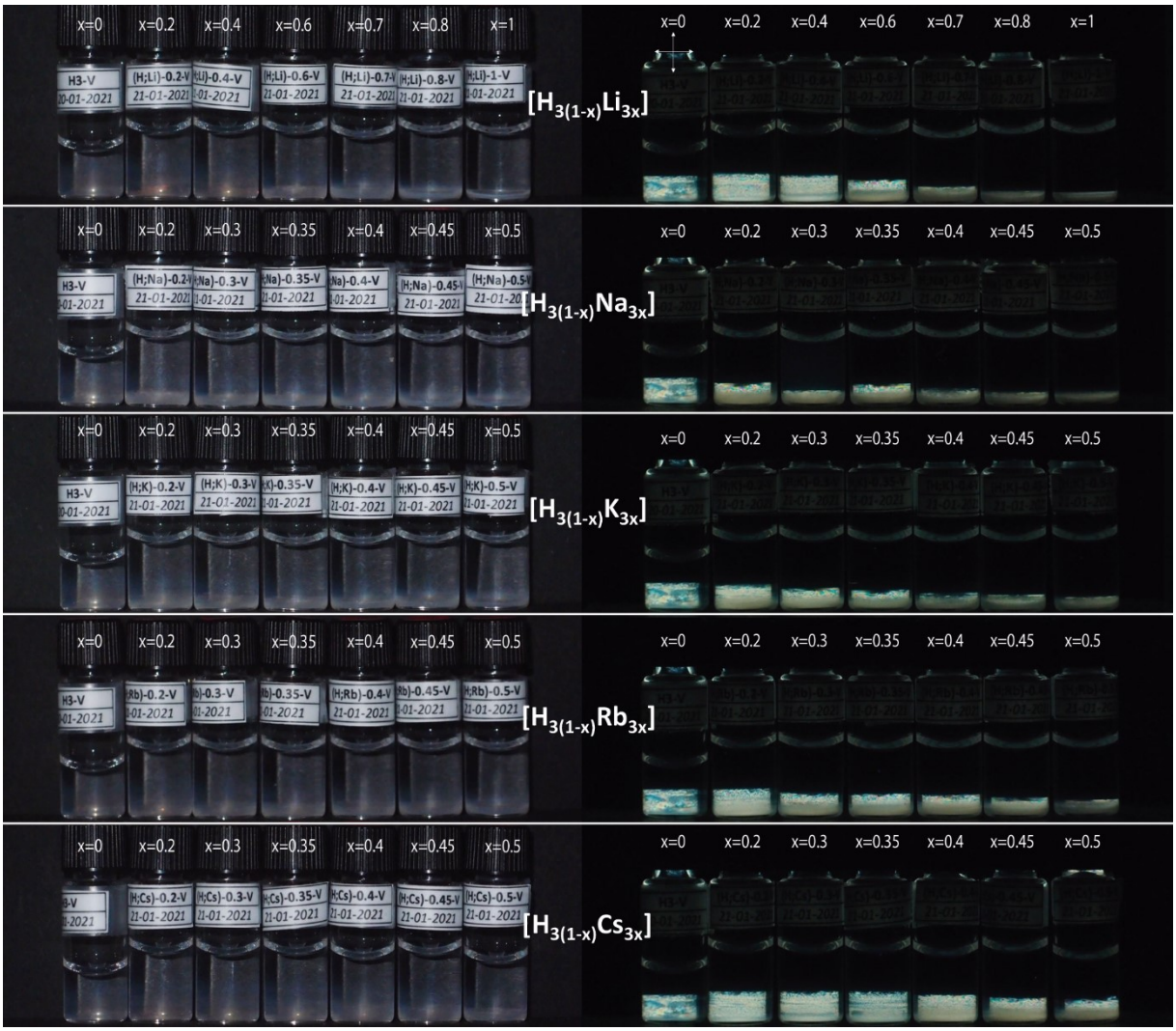

Figure SI 7. Photographs of five series of sample tubes observed in natural light (right) and between crossed polarizers (left). For each series, the $H_{3(1-x)}M_{3x}Sb_3P_2O_{14}$ nanosheet weight fraction is kept constant (0.33 wt %) but the x value corresponding to the alkali cation present increases from left to right: x = 0, 0.2, 0.4, 0.6, 0.7, 0.8 and 1 for Li^+ and x = 0, 0.2, 0.3, 0.35, 0.4, 0.45 and 0.5 for the rest of the cations (Na^+, K^+, Rb^+, Cs^+). The lamellar phase is clearly destabilized by the addition the different cations.

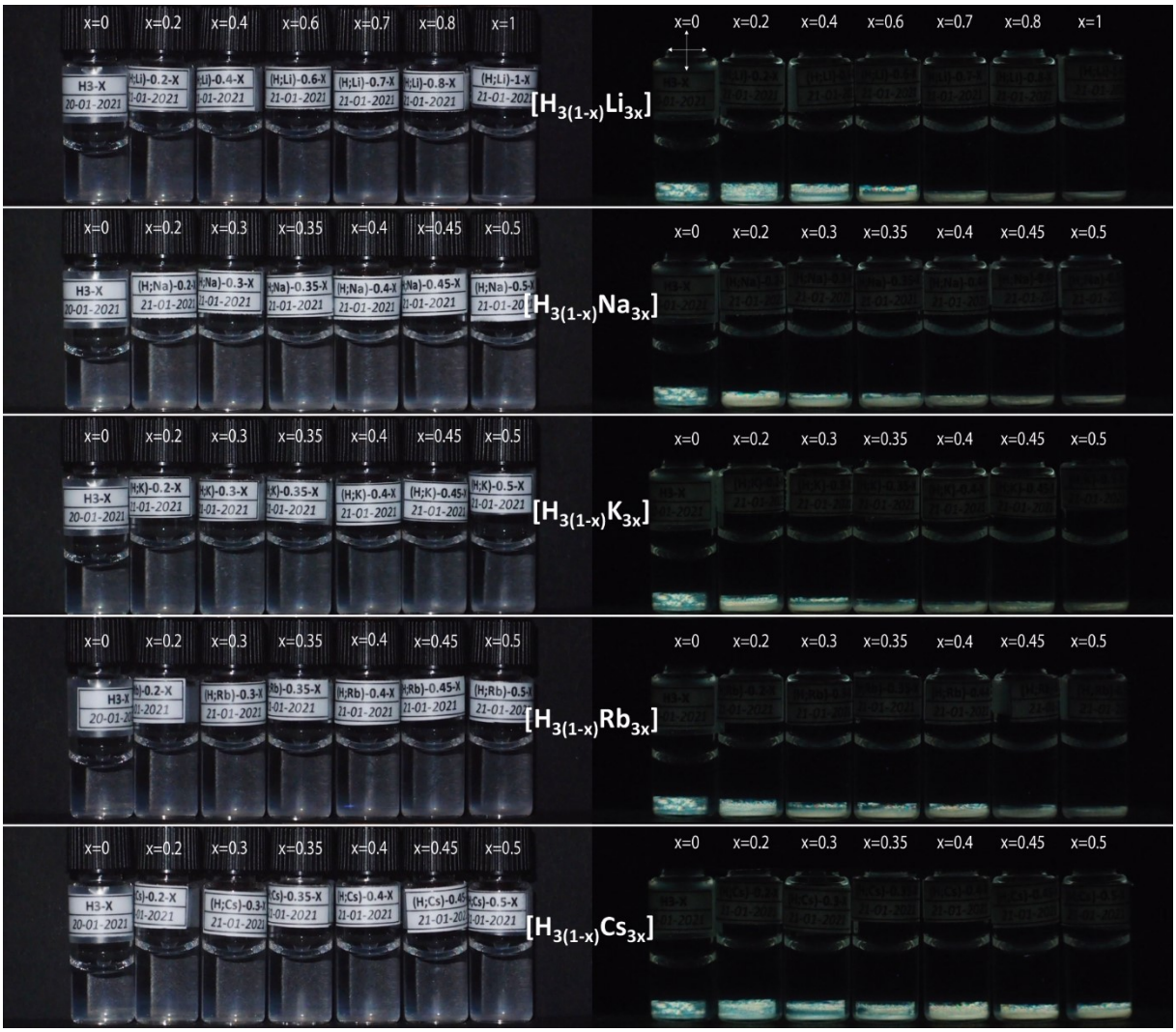

Figure SI 8. Photographs of five series of sample tubes observed in natural light (right) and between crossed polarizers (left). For each series, the $H_{3(1-x)}M_{3x}Sb_3P_2O_{14}$ nanosheet weight fraction is kept constant (0.17 %w/w) but the x value corresponding to the alkaline cation increases from left to right: x = 0, 0.2, 0.4, 0.6, 0.7, 0.8, and 1 for Li^+ and x = 0, 0.2, 0.3, 0.35, 0.4, 0.45, and 0.5 for the other cations (Na^+, K^+, Rb^+, Cs^+).

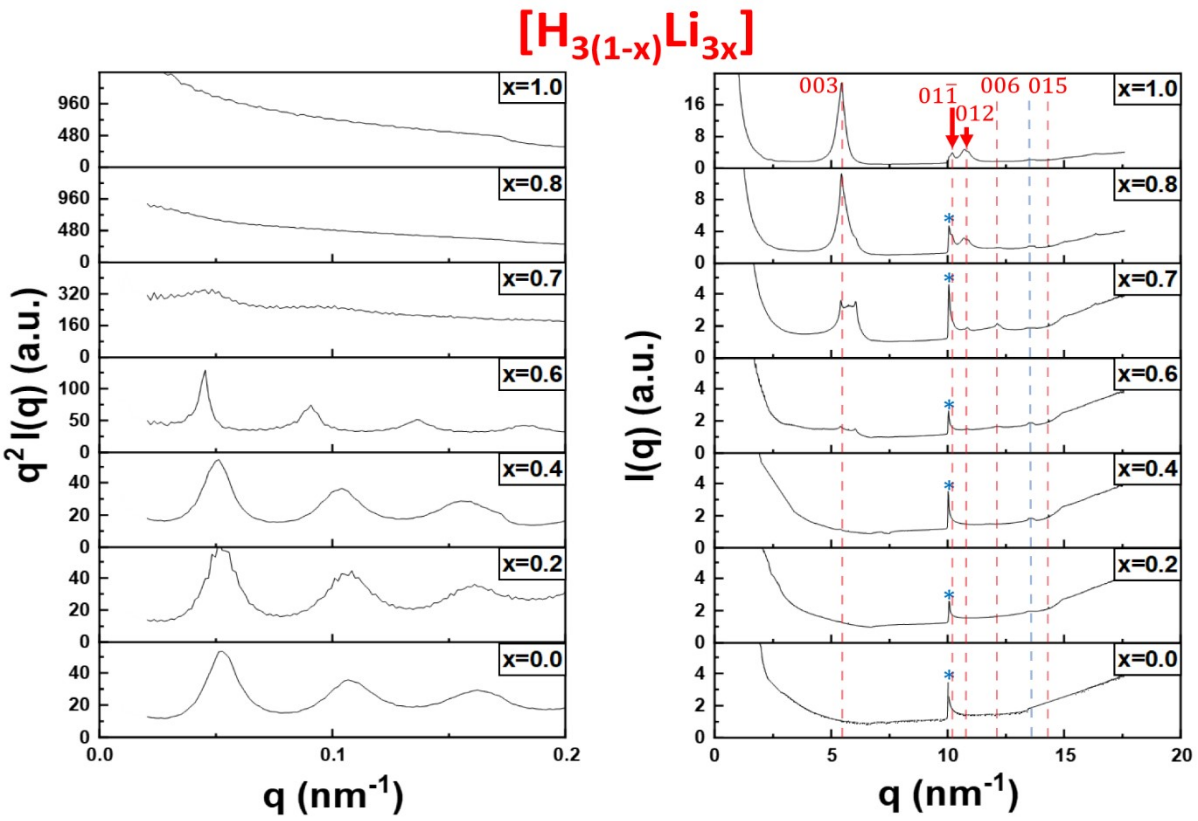

Figure SI 9. SAXS (left) and WAXS (right) patterns of the bottom phase of the samples shown in Figure 2 for the $[H_{3(1-x)}Li_{3x}]$ system.

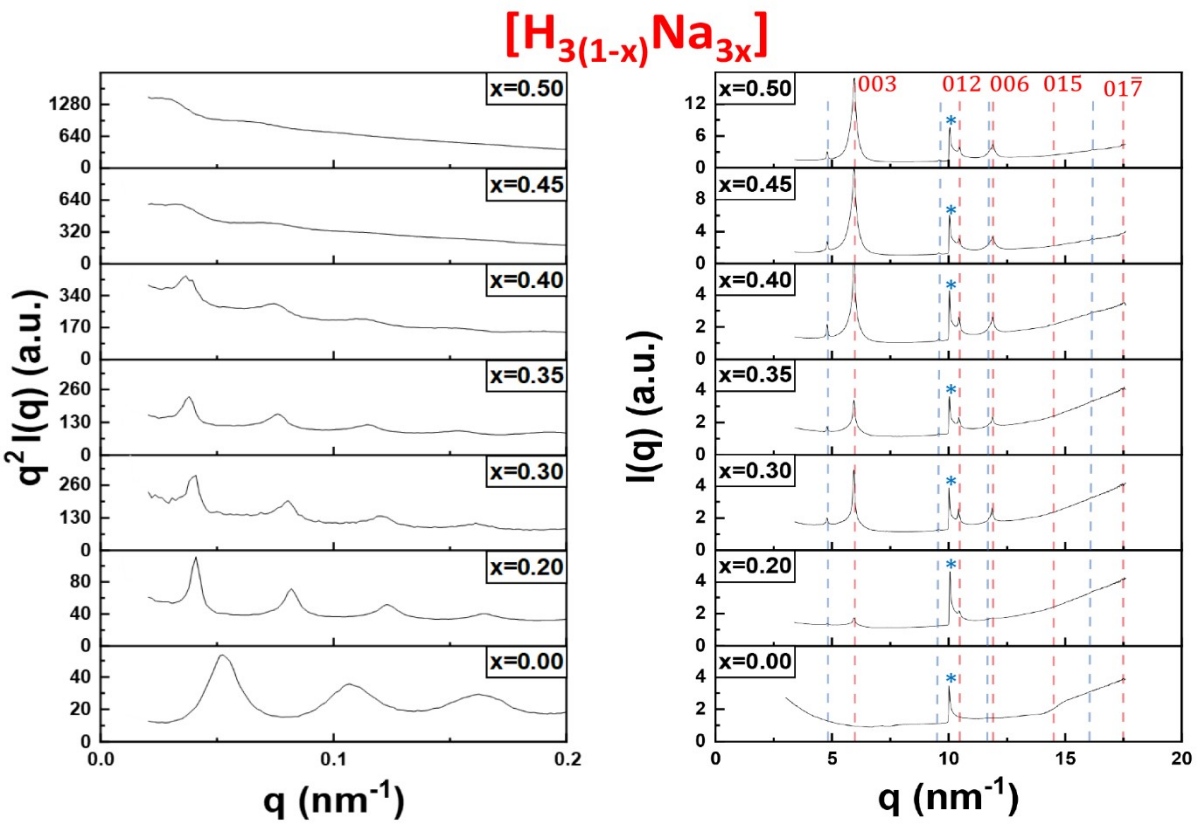

Figure SI 10. SAXS (left) and WAXS (right) patterns of the bottom phase of the samples shown in Figure 2 for the $[H_{3(1-x)}Na_{3x}]$ system.

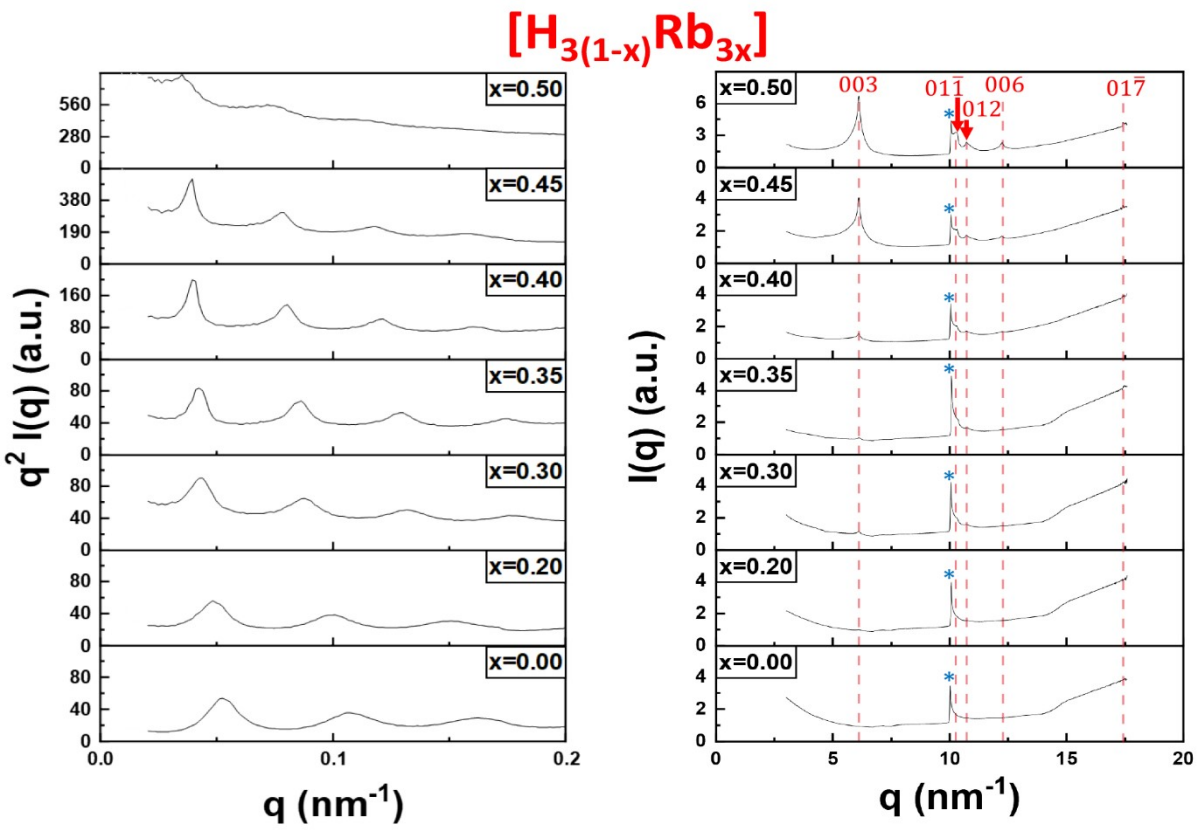

Figure SI 11. SAXS (left) and WAXS (right) patterns of the bottom phase of the samples shown in Figure 2 for the $[H_{3(1-x)}Rb_{3x}]$ system.

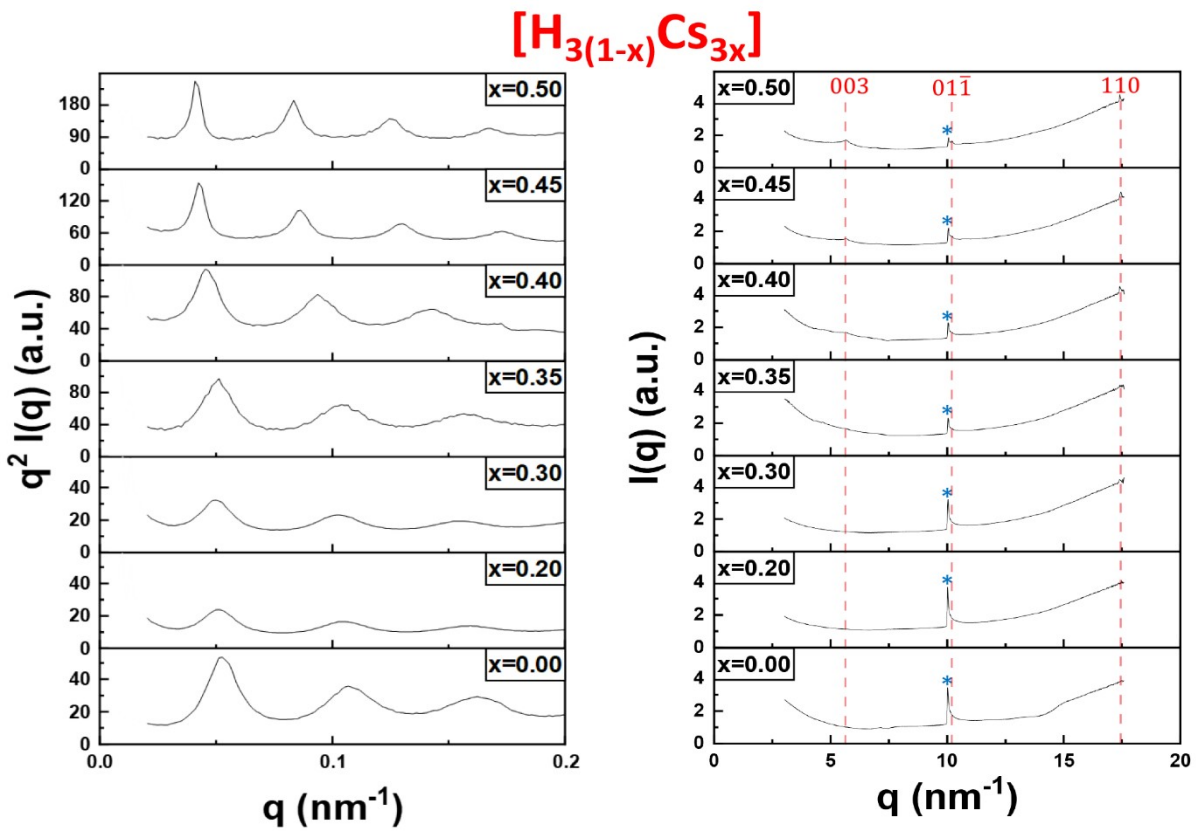

Figure SI 12. SAXS (left) and WAXS (right) patterns of the bottom phase of the samples shown in Figure 2 for the $[H_{3(1-x)}Cs_{3x}]$ system.

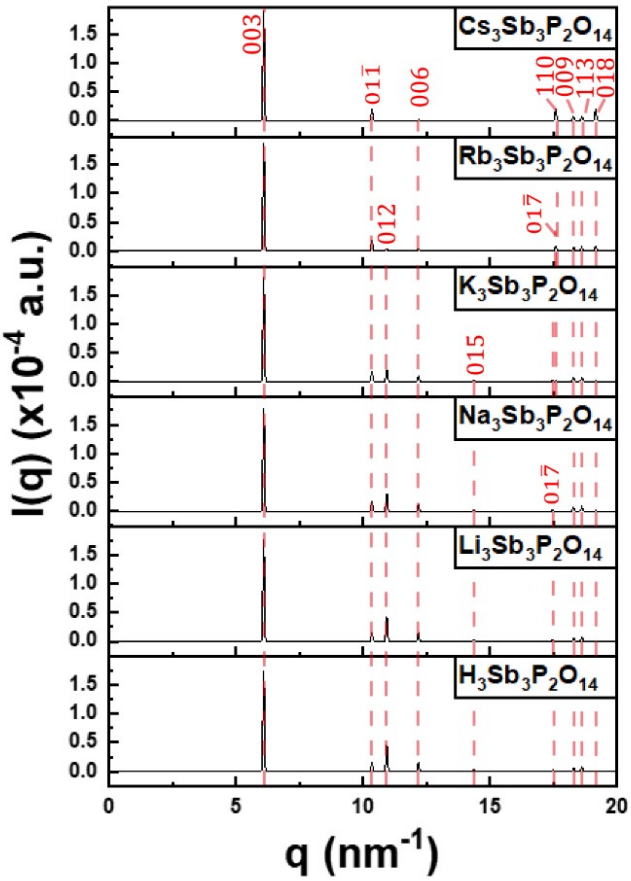

Figure SI 13. Simulated X-ray diffraction (XRD) patterns from the crystallographic structure of $K_3Sb_3P_2O_{14}$ by replacing potassium with protons or alkaline (Li, Na, Rb, Cs) cations.

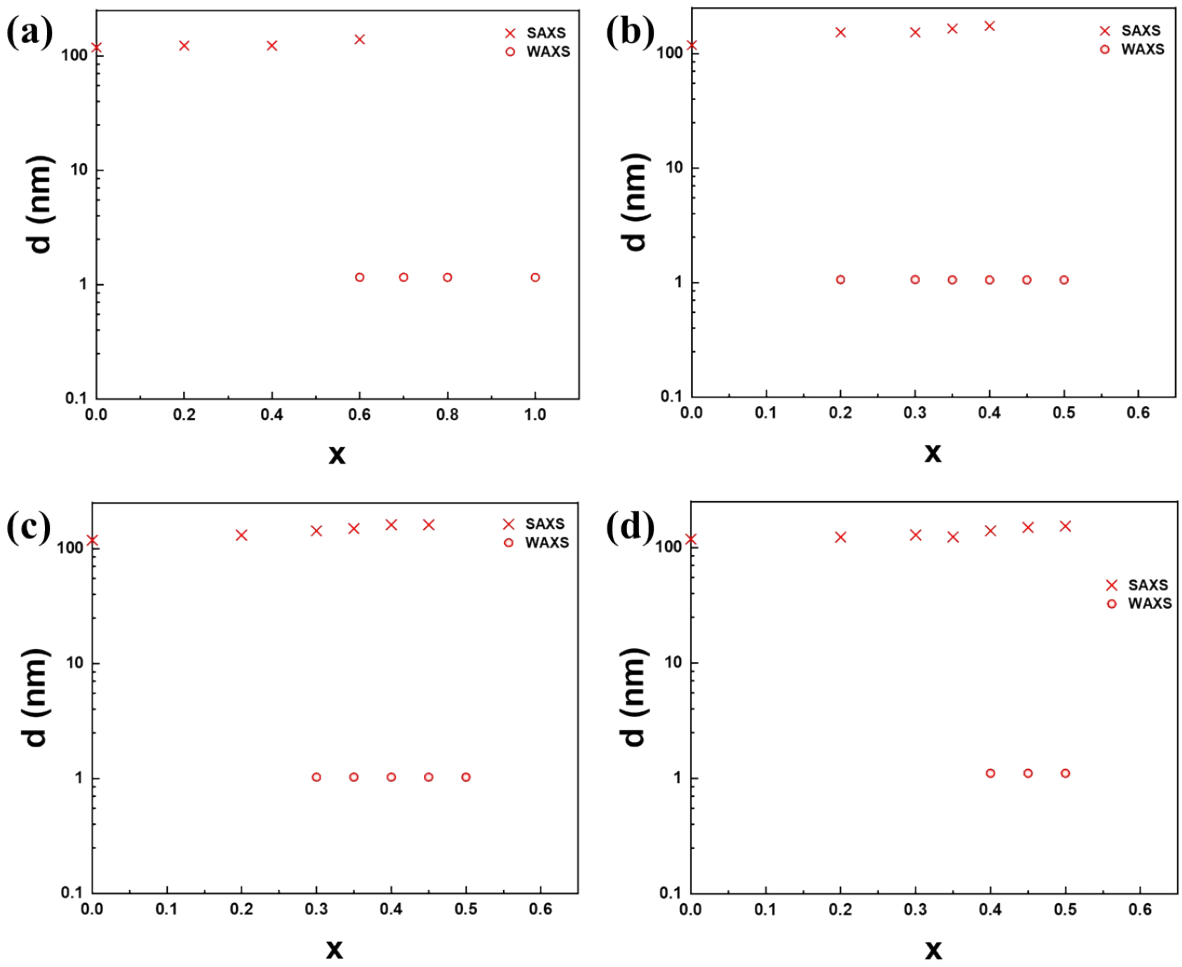

Figure SI 14. Dependence of the lamellar period on the cation exchange rate x for (a) $H_{3(1-x)}Li_{3x}Sb_3P_2O_{14}$, (b) $H_{3(1-x)}Na_{3x}Sb_3P_2O_{14}$, (c) $H_{3(1-x)}Rb_{3x}Sb_3P_2O_{14}$ and (d) $H_{3(1-x)}Cs_{3x}Sb_3P_2O_{14}$ samples.

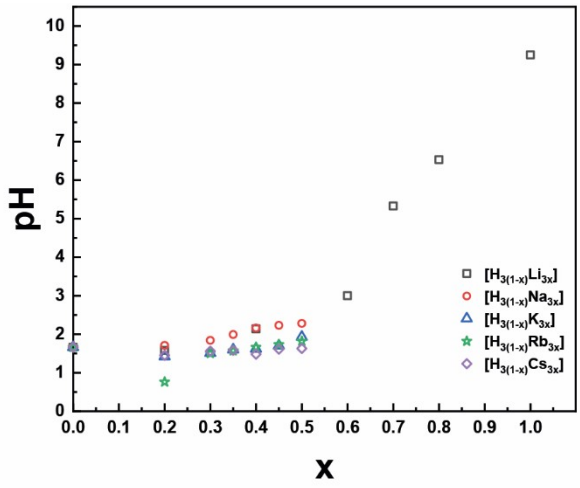

Figure SI 15. Dependance of the pH value on the cation exchange rate x for all series of samples shown in Figure 2 (with constant $H_3Sb_3P_2O_{14}$ weight fraction (1.65 %w/w)).

Fast swelling of $H_3Sb_3P_2O_{14}$ prepared by reverse cationic exchange of $M_3Sb_3P_2O_{14}$

- **$H_3Sb_3P_2O_{14}$ from $K_3Sb_3P_2O_{14}$**

Dry solid	Swelling in presence of water
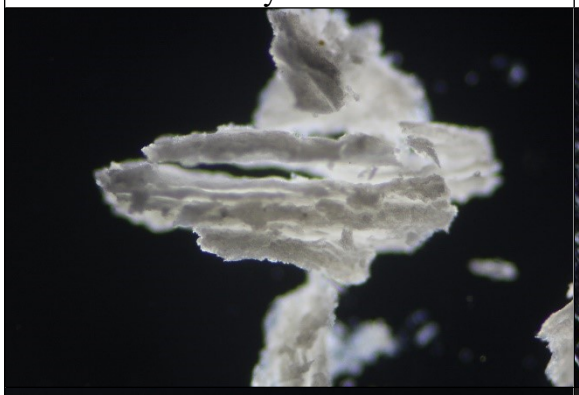	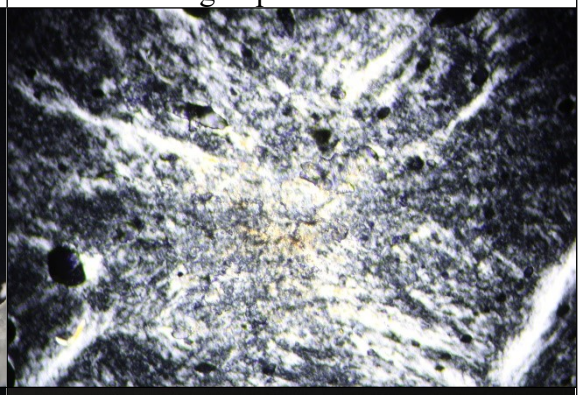
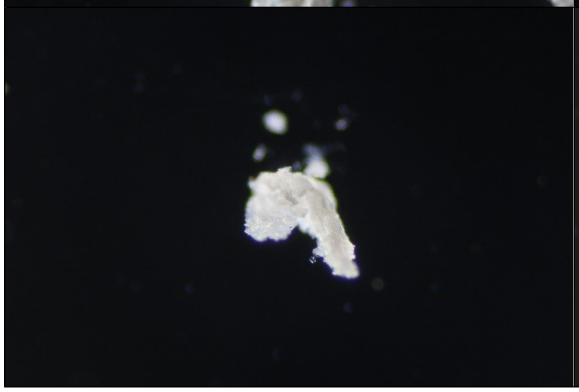	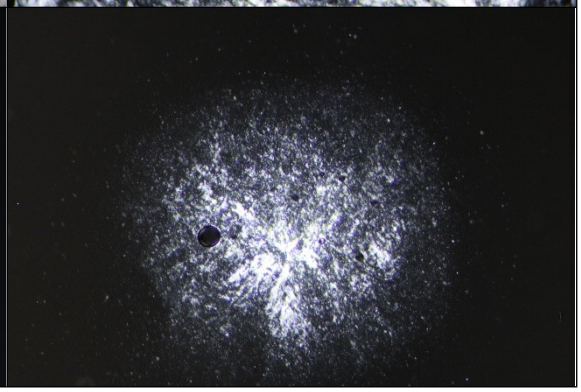

Table SI 1. Photographs of $H_3Sb_3P_2O_{14}$ prepared by reverse cationic exchange of $K_3Sb_3P_2O_{14}$, observed using an optical microscope with crossed polarizers with a magnification of 10. Left: dry synthesised solid; right: swelling in presence of water.

- **$H_3Sb_3P_2O_{14}$ from $Na_3Sb_3P_2O_{14}$**

Dry solid	Swelling in presence of water
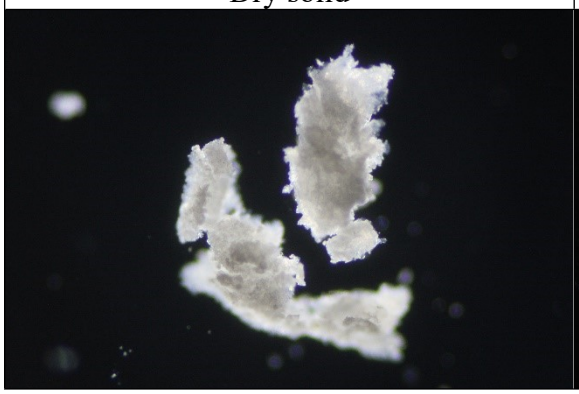	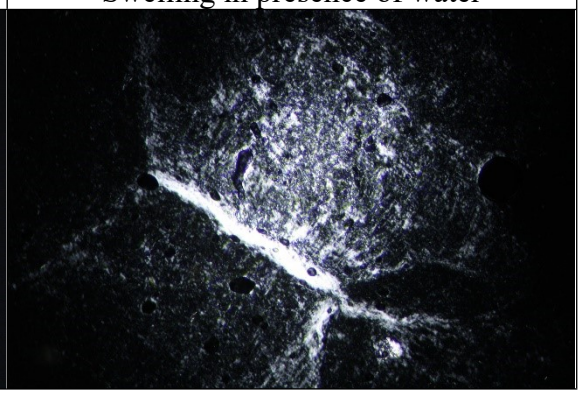

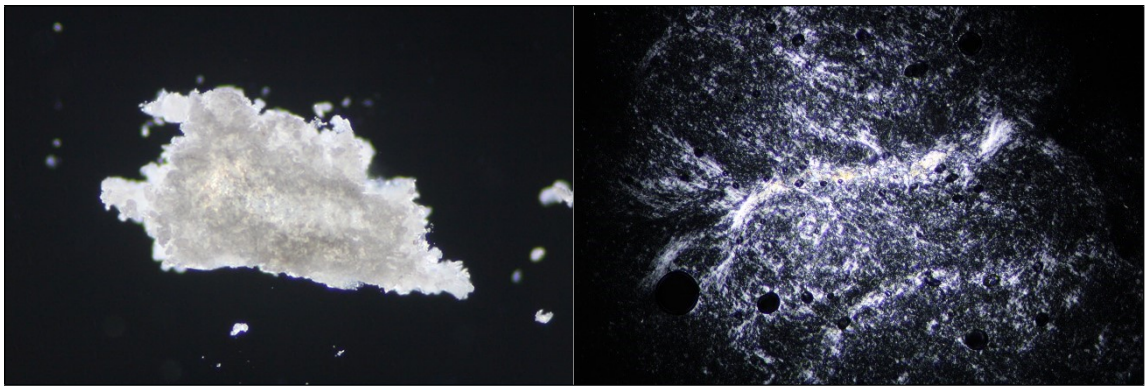

Table SI 2. Photographs of $H_3Sb_3P_2O_{14}$ prepared by reverse cationic exchange of $Na_3Sb_3P_2O_{14}$, observed using an optical microscope with crossed polarizers with a magnification of 10. Left: dry synthesised solid; right: swelling in presence of water.

- **$H_3Sb_3P_2O_{14}$ from $Rb_3Sb_3P_2O_{14}$**

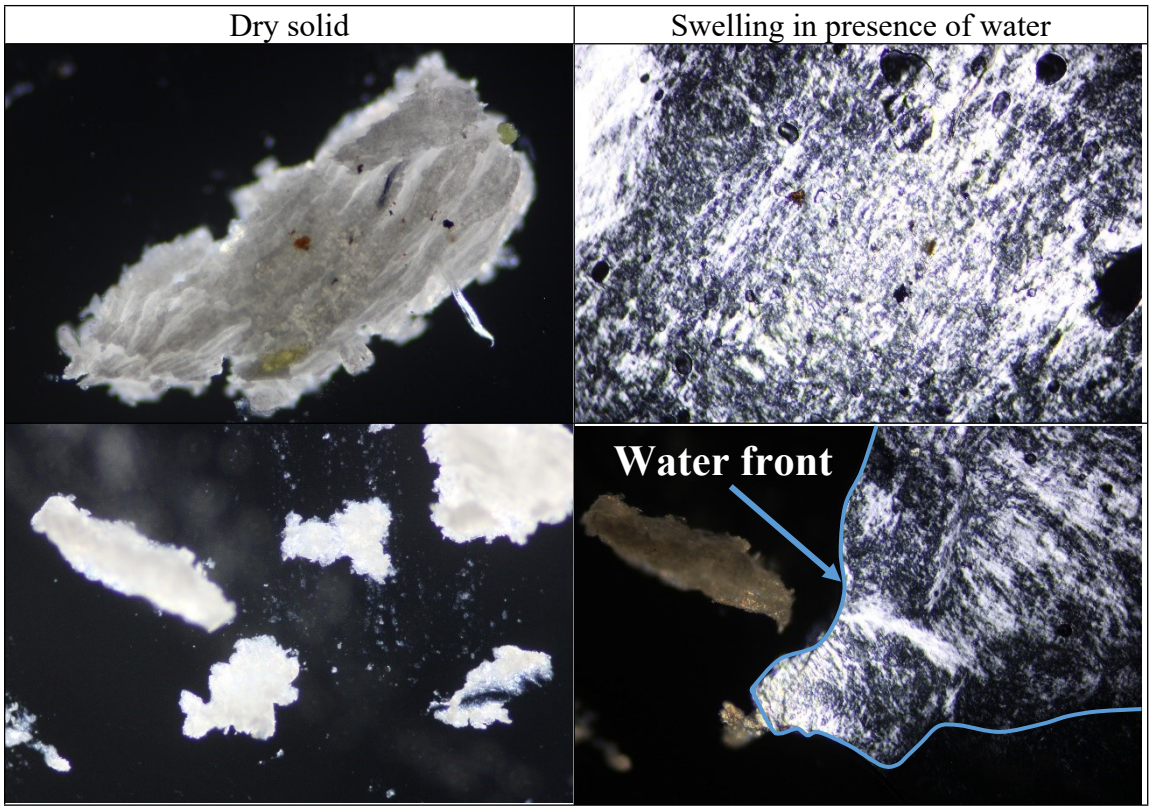

Table SI 3. Photographs of $H_3Sb_3P_2O_{14}$ prepared by reverse cationic exchange of $Rb_3Sb_3P_2O_{14}$, observed using an optical microscope with crossed polarizers with a magnification of 10. Left: dry synthesised solid; right: swelling in presence of water.

The fast swelling of the $H_3Sb_3P_2O_{14}$ phases recovered from $M_3Sb_3P_2O_{14}$ restacked materials showed the reversibility of the restacking process.

SI19: Lamellar Lennard-Jones potential

Let us consider the Lennard-Jones potential that combines van der Waals attraction and volume exclusion repulsion between two atoms at short distance r:

$$U(r) = \left(\frac{B}{r}\right)^{12} - \left(\frac{C}{r}\right)^{6} \qquad \textbf{SI 1}$$

Let us now generalize this potential towards two thin lamellae each with a given atomic density ρ (number of atoms per unit volume). The van der Waals interaction energy per unit area A between two parallel slabs of thickness h and distance d is obtained by straightforward integration of Eq. ($Ur = \left(\frac{B}{r}\right)^{12} - \left(\frac{C}{r}\right)^{6}$ **SI *1***) and reads:

$$\frac{U_{vdW}(d)}{A} = -\frac{A_L}{12\pi}\left[\frac{1}{d^2} - \frac{2}{(d+h)^2} + \frac{1}{(d+2h)^2}\right] \qquad \textbf{SI 2}$$

with $A_L = \pi^2\rho^2 C = A_c\phi_\perp^{\,2}$ (units J) which depends on the intrinsic Hamaker constant A_c of the colloidal material and the intralamellar packing fraction $\phi_\perp$. For the repulsive part we find similarly:

$$\frac{U_{rep}(d)}{A} = -\frac{B_L}{360\pi}\left[\frac{1}{d^8} - \frac{2}{(d+h)^8} + \frac{1}{(d+2h)^8}\right] \qquad \textbf{SI 3}$$

with $B_L = \pi\rho^2 B = B_c\phi_\perp^{\,2}$ (units Jm^6) and B_c an constant pertaining to the colloidal material. Combining the two and Taylor expanding for $h/D \ll 1$ we find a Lennard-Jones (LJ) type potential modified for the case of two thin lamellae of thickness h interacting at a distance $d \gg h$:

$$\frac{U_{LLJ}(d)}{A} = -\frac{A_L h^2}{2\pi d^4} + \frac{B_L h^2}{5\pi d^{10}} \qquad \textbf{SI 4}$$

The minimum of the potential occurs at $d^* = (B_c/A_c)^{1/6}$ which is fixed for a given colloidal material. The minimum of the potential is given by $U^*_{mLJ}/A = -3A_c\phi_\perp^{\,2}h^2/10\pi(d^*)^4$ which is proportional to the square of the intralamellar packing fraction $\phi_\perp$. Similar to the conventional LJ potential, the "lamellar" version (LLJ) can be reexpressed in a rescaled form:

$$\frac{U_{LLJ}(d)}{A} = \varepsilon\phi_\perp^{\,2}\left[2\left(\frac{d^*}{d}\right)^{10} - 5\left(\frac{d^*}{d}\right)^{4}\right] \qquad \textbf{SI 5}$$

with amplitude

$\varepsilon = A_c h^2/10\pi(d^*)^4 > 0$

The LLJ potential reaches a minimum $-\varepsilon\phi_\perp^{\,2}$ when $d = d^*$.

SEM-EDX analysis of $M_3Sb_3P_2O_{14}$ restacked phases

Figure SI 16 shows the M/Sb atomic ratio calculated from the EDX atomic composition analysis of restacked $M_3Sb_3P_2O_{14}$ phases (x=1), where M = Cs, K, Na or Rb. EDX analysis were not performed on $Li_3Sb_3P_2O_{14}$ because lithium is too light to be detected by EDX. The expected M/Sb ratio is equal to 1.

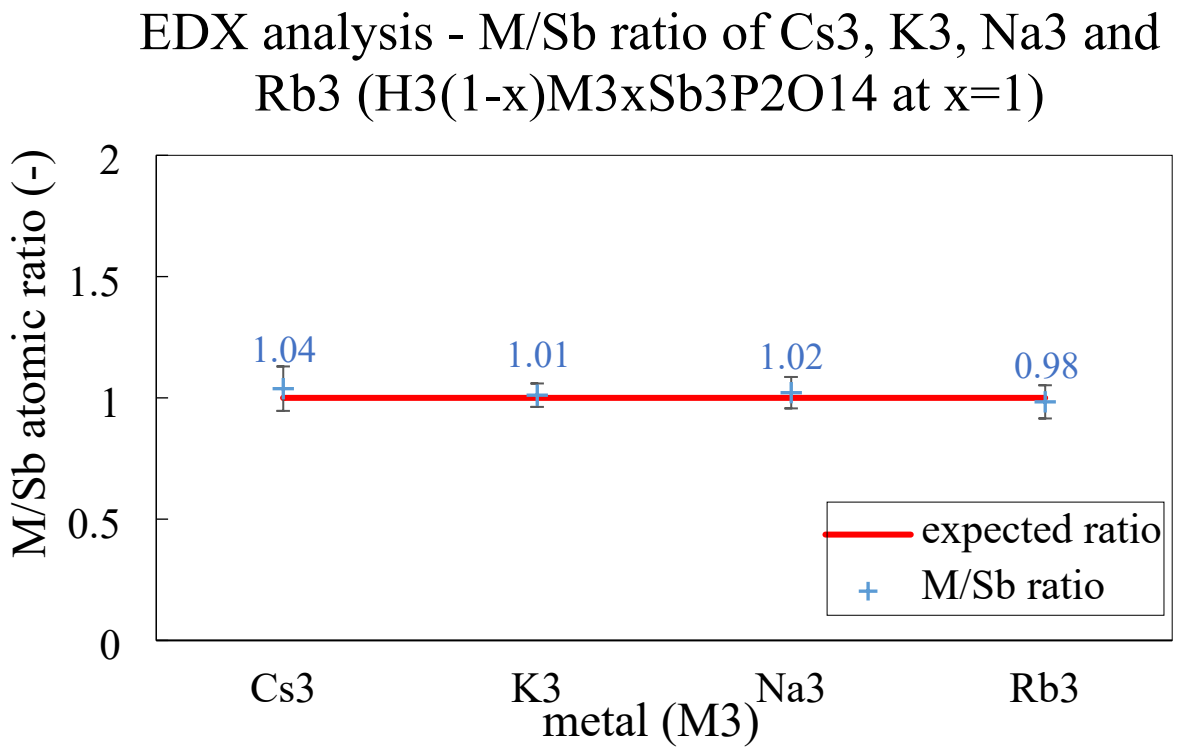

Figure SI16. EDX analysis of $Cs_3Sb_3P_2O_{14}$ (Cs3), $K_3Sb_3P_2O_{14}$ (K3), $Na_3Sb_3P_2O_{14}$ (Na3), and $Rb_3Sb_3P_2O_{14}$ (Rb3) (x=1). Calculation of M/Sb atomic ratio (where M = Cs, K, Na or Rb).

The EDX analysis confirmed the expected value of x = 1 for restacked $M_3Sb_3P_2O_{14}$ phases.